

Wall Thickness and Radial Breathing Modes of Single-Walled Carbon Nanotubes

R. C. Batra

Fellow ASME
e-mail: rbatra@vt.edu

S. S. Gupta

e-mail: ssgupta@vt.edu

Department of Engineering Science and
Mechanics,
M/C 0219 Virginia Polytechnic Institute
and State University,
Blacksburg, VA 24061

We postulate that an equivalent continuum structure (ECS) of a single-walled carbon nanotube (SWCNT) is a hollow cylinder with mean radius and length equal to that of the SWCNT, and find the thickness of the ECS so that its mechanical response in free vibrations is the same as that of the SWCNT. That is, for mechanical deformations, the ECS is energetically equivalent to the SWCNT. We use MM3 potential to study axial, torsional, radial breathing and bending vibrations of several traction free–traction free SWCNTs of different helicities and diameters and compare them with the corresponding vibrational modes and frequencies of traction free–traction free ECSs obtained by using the three-dimensional linear elasticity theory and the finite element analysis (3D-FEA). The consideration of free ends eliminates the effects of boundary conditions and avoids resolving equivalence between boundary conditions in the analyses of SWCNTs and their ECSs. It is found that the wall thickness of the ECS (and hence of a SWCNT) is ~ 1 Å and Young's modulus of the material of the ECS (and hence of the SWCNT) is ~ 3.3 TPa. Both quantities are independent of the helicity and the diameter of the SWCNT. We also study radial breathing mode (RBM) vibrations with the molecular dynamics and the 3D-FEA simulations, and compare them with experimental findings. Accuracy in the assignment of spectral lines for RBMs in the Raman spectroscopy is discussed.

[DOI: 10.1115/1.2965370]

1 Introduction

Since their discovery by Iijima [1] there has been significant interest in characterizing the mechanical properties of both single-walled and multiwalled carbon nanotubes (SWCNTs and MWCNTs, respectively). An inherent difficulty in completing this task is assigning a thickness to the nanotube. Nearly all studies to date have assumed that a SWCNT can be obtained by rolling a graphene sheet into a cylindrical tube about a vector with components (m, n) , and the response of a SWCNT is equivalent to that of a continuum structure (see Fig. 1) undergoing the same deformations as the SWCNT. In these studies the thickness of a SWCNT varies from 0.66 Å to 6.8 Å. While most studies have assumed the wall thickness to be 3.4 Å (the interlayer separation distance of graphene sheets in the bulk graphite) some works have taken it to be less than 3.4 Å [2–12] and a few have taken it to be 6.8 Å [12,13]. This large variation in thickness gives values of Young's modulus ranging from 0.27 TPa for MWCNTs [14] to 5.5 TPa for SWCNTs [2].

The mechanical properties of ECSs can be used to deduce the effective elastic moduli of SWCNTs-reinforced composites from those of their constituents and their volume fractions by using a homogenization technique; see, e.g., Ref. [15]. Good agreement between the computed effective moduli of the composite and the measured ones will validate the mechanical properties of ECSs and hence of SWCNTs. This is not pursued here.

Raman spectroscopy is a reliable technique to identify SWCNTs experimentally. A peak corresponding to a radial breathing mode (RBM) is a significant spectral line observed during experiments. The identification of SWCNTs and the determination of their RBM frequencies using quantum mechanical simulations and spectroscopy are described in Refs. [16–19].

Here we analyze the normal mode vibrations of traction free–

traction free SWCNTs of various helicities and diameters using MM3 potential and compare their vibrational modes and frequencies with the corresponding ones for an ECS derived by using the three-dimensional theory of elasticity and the finite element analysis (3D-FEA) to ascertain values of the thickness and the elastic moduli of the ECS and hence of the SWCNT. An advantage of the 3D-FEA is that it incorporates both in-plane and out-of-plane deformations, and provides more realistic deformations of the continuum tube than those obtained by using either a beam or a shell theory.

Whereas the MM3 (and other) potential includes the effect of van der Waals forces, which describe the long range interactions between unbonded atoms, the classical elasticity theory is local. A good agreement between predictions from molecular dynamics (MD) simulations and 3D-FEA using linear elasticity theory will imply that van der Waals forces play a less significant role than that played by forces between bonded atoms. One can use such comparisons between the results of the MD and the 3D-FE simulations to delimit the class of deformations for which the effects of van der Waals forces are negligible.

We describe below the details of the MD and 3D-FE simulations, and the conclusions of our work.

2 Molecular Dynamics, Three-Dimensional Elasticity, and Finite Element Simulations

The MM3 [20] Class II pairwise potential with both higher-order expansions and cross-terms and Type 2 (alkene) carbon atoms with a bond length of ~ 1.42 Å is used to model SWCNTs in the computer code TINKER [21]. This potential is appropriate for carbon nanotubes due to the similarity between graphitic bonds in the nanotube and the aromatic protein structures for which the potential is constructed. The MM3 potential is given as Eq. (1) in which U_s , U_θ , and U_ϕ are the primary bond deformation terms accounting, respectively, for the change in the bond length, the change in the angle between adjoining bonds, and the twisting of bonds with respect to the one to which it is bonded. The potential U_s has terms that are quadratic, cubic, and quartic in the change of

Contributed by the Applied Mechanics Division of ASME for publication in the JOURNAL OF APPLIED MECHANICS. Manuscript received November 15, 2007; final manuscript received March 11, 2008; published online August 20, 2008. Review conducted by Yonggang Huang.

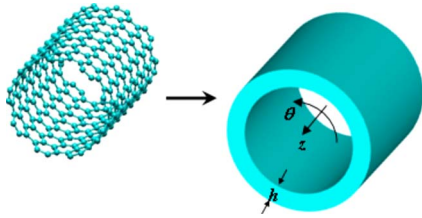


Fig. 1 Cylindrical tube equivalent in mechanical response to a SWCNT

bond lengths, and hence is asymmetric with respect to the decrease and increase in the bond length. U_{vdW} is the potential of nonbonded van der Waals forces, and its expression involving terms $(r_v/r)^6$ and $\exp(-12r/r_v)$ is different from that in the Lennard–Jones potential; U_{vdW} is negligible for r_v/r greater than 2 where r_v is a material parameter and r is the bond length. U_s , U_θ and $U_{\phi s}$ are potentials due to interactions among stretching and bending deformations, and between stretching and twisting deformations. $U_{\theta\theta'}$ represents the interactions between different bending modes. Parameters r , θ , and ϕ used in Eq. (1) are shown in Fig. 2. A subscript, e , on a variable signifies its value in the configuration of minimum potential energy. The total energy of a body equals the sum of the potentials of all atoms in the body (the indices i and j in Eq. (1) range over bonded atoms, and the index k over all atoms).

$$U = \sum_i \sum_j (U_s + U_\theta + U_\phi + U_{s\theta} + U_{\phi s} + U_{\theta\theta'}) + \sum_i \sum_k U_{vdW}$$

$$U_s = 71.94K_s(r - r_e)^2 \left[1 - 2.55(r - r_e) + \left(\frac{7}{12}\right)2.55(r - r_e)^2 \right]$$

$$U_\theta = 0.021914K_\theta(\theta - \theta_e)^2 \left[1 - 0.014(\theta - \theta_e) + 5.6(10)^{-5}(\theta - \theta_e)^2 - 7.0(10)^{-7}(\theta - \theta_e)^3 + 9.0(10)^{-10}(\theta - \theta_e)^4 \right]$$

$$U_\phi = (V_1/2)(1 + \cos \phi) + (V_2/2)(1 - \cos 2\phi) + (V_3/2)(1 + \cos 3\phi)$$

$$U_{s\theta} = 2.51118K_{s\theta}[(r - r_e) + (r' - r'_e)](\theta - \theta_e)$$

$$U_{\phi s} = 11.995(K_{\phi s}/2)(r - r_e)(1 + \cos 3\phi)$$

$$U_{\theta\theta'} = -0.021914K_{\theta\theta'}(\theta - \theta_e)(\theta' - \theta'_e) \quad \text{and}$$

$$U_{vdW} = \epsilon_e \left\{ -2.25(r_v/r)^6 + 1.84(10)^5 \exp[-12.0(r/r_v)] \right\} \quad (1)$$

The values of constants K_s , K_θ , V_1 , V_2 , V_3 , ϵ_e , r_v , $K_{s\theta}$, $K_{\phi s}$, and $K_{\theta\theta'}$ are given in Ref. [20]. The potential includes contributions from bond stretching, bending deformations that change angles between adjoining bonds, torsion, and van der Waals forces. Moreover, it also accounts for interactions between stretching and bending, and stretching and twisting. Contributions from different terms in Eq. (1) for axial tensile and compressive deformations plotted in Fig. 9 of Ref. [22] reveal that in axial deformations of a (16,0) SWCNT the angle bend mode of deformation makes a significant contribution to the total energy of deformation. Also, deformations due to van der Waals forces contribute more to the total energy of deformation during compressive deformations than that during tensile deformations. The stretching mode of deforma-

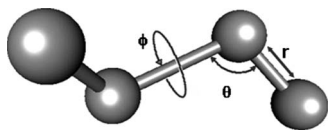


Fig. 2 Depictions of variables r , θ , and ϕ used in the MM3 potential

tion contributes most to the energy of deformation during axial tensile deformations. However, during axial compressive deformations, contributions from angle mode and bond stretching terms are nearly equal to each other.

The following procedure is adopted to analyze the vibrations of free-free SWCNTs; here free-free implies that the end surfaces of a SWCNT and its ECS are traction free. These boundary conditions can be achieved in a laboratory more readily than those of either simply supported or clamped edges. A SWCNT is first relaxed to find the minimum energy configuration at room temperature to within 0.001 kcal/mol/Å rms without using any cut-off distance. Thus each atom of the SWCNT can potentially influence the deformations of other atoms in the tube. However, depending on the value of r_v in Eq. (1) for the van der Waals force potential, the van der Waals force between two atoms separated by three or four times the distance between two bonded atoms is negligible as compared with other forces acting on an atom. It is ensured that each tube in the relaxed configuration has an aspect ratio (length/diameter) of about 15, so that when studying vibrations of its ECS the transverse inertia effects, which couple the thickness, Young's modulus, Poisson's ratio, and the frequency of axial oscillations, are minimized. Furthermore, a high aspect ratio satisfies the criterion [23] $l_e/j \gg r_e$ for identifying the frequency of a RBM equivalent to that of an infinitely long tube (e.g., periodic boundary conditions on the unit cell), where j is the number of half-wavelengths along the longitudinal direction, and l_e and r_e are, respectively, the length and the mean radius of the relaxed SWCNT. The length l_e is the Euclidean distance between planes of atoms at the two end faces of the relaxed tube, and the radius r_e of an (m,n) SWCNT is given by $r_e = 1.1026 a_e(m^2 + n^2 + mn)^{1/2}$ where a_e is the bond length in its relaxed configuration. Tubes with $m=n$ are called armchair, those with either $n=0$ or $m=0$ are called zigzag, and others are called chiral.

The VIBRATE module in computer code TINKER is used to find frequencies of axial, torsional, radial breathing, and bending modes of vibrations of free-free SWCNTs of different diameters and helicities. This module computes the Hessian of the system by finding second-order derivatives of the MM3 potential with respect to variables appearing in the expression for the potential, and then diagonalizes the mass weighted Hessian to compute the eigenvalues and eigenvectors of normal modes. Frequencies computed using TINKER are equated to those of the corresponding modes of vibration of the ECS using the three-dimensional linear elasticity theory for isotropic materials and the FE computer code ABAQUS [24] with 20-node solid elements and one element through the thickness. The mean diameter and the length of the continuum cylindrical tube are taken to equal to those of the corresponding relaxed SWCNT.

Young's modulus (E) and the shear modulus (G) for a SWCNT are obtained by equating the frequencies of axial (ω_{iA}) and torsional modes (ω_{iT}) of vibration of a SWCNT computed with MD simulations and the 3D-FEA of the ECS. Frequencies, in rad/s, of free-free tubes from the elasticity theory [23] are given by

$$\omega_{iA} = i\pi(l_e)^{-1}(E/\rho)^{1/2} \quad \text{and} \quad \omega_{iT} = i\pi(l_e)^{-1}(G/\rho)^{1/2} \quad \text{for } i = 1, 2, 3, \dots \quad (2)$$

where ω_{iA} and ω_{iT} are, respectively, the frequency of the i th axial and torsional modes of vibration of the ECS. The mass density (ρ) is obtained by dividing the total mass of carbon atoms in the SWCNT by the volume of corresponding ECS with thickness as a variable. Poisson's ratio (ν) of the material of the ECS is expressed in terms of values of the i th frequencies of the axial and the torsional vibrations obtained with the MD simulations as

$$\nu = 0.5(\omega_{iA}/\omega_{iT})^2 - 1 \quad (3)$$

which holds because $E=2G(1+\nu)$ for an isotropic linear elastic material.

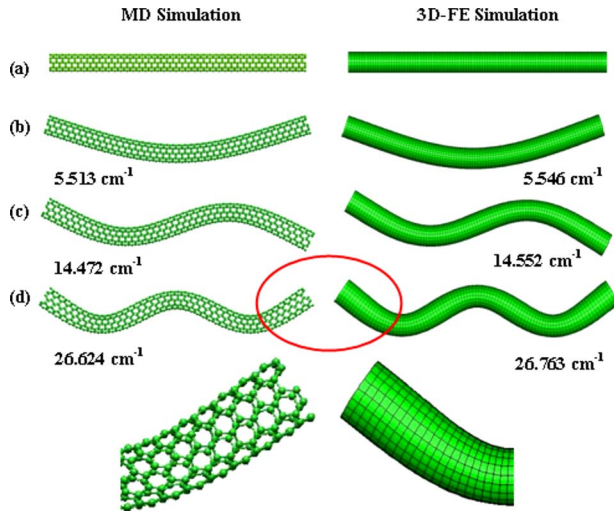


Fig. 3 Vibrational modes of free-free (5,5) SWCNT: (a) relaxed tube, (b) first bending mode, (c) second bending mode, and (d) third bending mode with zoomed ends indicating the presence of out-of-plane deformations

We note that a necessary condition for the existence of an ECS is that the frequency of the i th axial (or torsional) mode of vibration of a SWCNT derived from the MD simulations equals i times that of the first mode.

The thickness of the ECS is varied until the frequencies of the first three modes of axial, torsional, and bending modes from the MD simulations and the 3D-FEA match with each other within the prescribed tolerance of 1.0%. It should be noted that the variation in thickness does *not* alter the ratio (E/G); therefore, the bending mode frequency determines the termination of the iteration process for finding the thickness of the ECS. A good match between frequencies of the RBMs validates the thickness of the ECS.

3 Results and Discussion

Simulations for several SWCNTs have been carried out to delineate the dependence of material moduli and the wall thickness on their diameters and helicities. The afore-stated procedure gave a wall thickness of ~ 1 Å. For this value of the wall thickness, frequencies of vibrational modes from MD and 3D-FE simulations differed from each other by less than 1.0%. Figures 3(b)–3(d) illustrate the mode shapes and the corresponding frequencies from MD and 3D-FE simulations for bending modes for the (5,5) SWCNT. It can be observed that the flaring (i.e., out-of-plane deformations) at the end faces of the SWCNT marked in red circles in Fig. 3(d) is captured in the 3D-FEA but not in a beam or in a shell model of a SWCNT. For a SWCNT of small aspect ratio, the energy of deformation associated with end flaring may be significant. Tables 1 and 2 list the number of carbon atoms in a

Table 1 SWCNT parameters, frequencies (Hz/speed of light in cm/s) from molecular dynamics (MD) and finite element (FE) simulations, and values of elastic moduli

Tube	Geometry/atoms/ finite elements (r_0, l_0) (Å) ^a (r_e, l_e) (Å) ^a n_C, N^e	No. ^f	MD (MM3 potential)			$\langle E \rangle$ (TPa) $\langle \nu \rangle$ $\langle G \rangle$ (TPa)	3D-FEA % error with respect to MD results		
			T^b (cm ⁻¹)	A^c (cm ⁻¹)	B^d (cm ⁻¹)		T^b	A^c	B^d
(5,0)	(1.957, 59.640)	1	37.546	58.006	9.823	3.182	0.165	0.207	0.657
	(1.869, 55.425)	2	74.994	115.842	25.855	0.193	0.043	0.131	0.181
	280, 660	3	112.243	173.311	47.694	1.330	0.178	0.001	0.288
(5,5)	(3.390, 103.299)	1	22.270	33.730	5.513	3.271	0.009	0.151	0.595
	(3.222, 97.043)	2	44.541	67.384	14.472	0.144	0.011	0.076	0.550
	840, 2037	3	66.818	100.878	26.624	1.430	0.022	0.054	0.519
(10,0)	(3.915, 119.280)	1	18.732	29.633	4.802	3.401	0.053	0.135	0.249
	(3.716, 112.969)	2	37.464	59.218	12.589	0.251	0.053	0.162	0.269
	1120, 2712	3	56.161	88.698	23.123	1.361	0.011	0.210	0.302
(9,6)	(5.119, 167.120)	1	13.622	20.893	3.167	3.317	0.044	0.115	0.095
	(4.856, 158.100)	2	27.244	41.753	8.355	0.175	0.048	0.079	0.143
	2052, 5056	3	40.866	62.542	15.462	1.422	0.047	0.021	0.187
(8,8)	(5.425, 164.787)	1	13.833	21.161	3.433	3.294	0.014	0.132	0.464
	(5.146, 155.261)	2	27.667	42.284	9.006	0.167	0.011	0.090	0.464
	2144, 5115	3	41.503	63.321	16.557	1.411	0.007	0.011	0.451
(14,2)	(5.911, 182.253)	1	12.282	19.276	3.075	3.367	0.008	0.119	0.033
	(5.606, 172.808)	2	24.561	38.522	8.071	0.229	0.024	0.130	0.074
	2584, 6228	3	36.840	57.710	14.846	1.369	0.027	0.160	0.114
(9,9)	(6.103, 184.463)	1	12.319	18.902	3.076	3.296	0.016	0.132	0.453
	(5.787, 173.879)	2	24.637	37.769	8.069	0.174	0.024	0.093	0.407
	2700, 6612	3	36.956	56.562	14.825	1.403	0.022	0.027	0.396
(16,0)	(6.264, 191.700)	1	11.633	18.329	2.943	3.360	0.000	0.126	0.271
	(5.939, 181.303)	2	23.263	36.631	7.719	0.239	0.009	0.148	0.271
	2880, 6878	3	34.891	54.871	14.185	1.356	0.020	0.184	0.288
(10,10)	(6.780, 204.139)	1	11.101	17.077	2.788	3.297	0.027	0.129	0.393
	(6.429, 192.503)	2	22.202	34.124	7.309	0.180	0.023	0.100	0.368
	3320, 8106	3	33.304	51.104	13.422	1.396	0.021	0.041	0.356

^a r and l are the radius and the length of a SWCNT, and subscripts 0 and e refer to the initial and the relaxed configurations, respectively.

^bTorsional mode.

^cAxial mode.

^dBending mode.

^e n_C and N are, respectively, the number of carbon atoms in the SWCNT, and the number of 20-node hexahedral elements into which the equivalent continuum tube is discretized.

^fMode number.

Table 2 SWCNT parameters, frequencies (Hz/speed of light in cm/s) from molecular dynamics (MD) and finite element (FE) simulations, and values of elastic moduli

Tube	Geometry/atoms/ finite elements (r_0, l_0) (Å) ^a (r_e, l_e) (Å) ^a n_C, N ^e	No. ^f	MD (MM3 potential)			$\langle E \rangle$ (TPa)	3D-FEA [% error with respect to MD results		
			T ^b (cm ⁻¹)	A ^c (cm ⁻¹)	B ^d (cm ⁻¹)	$\langle \nu \rangle$ (TPa)	T ^b	A ^c	B ^d
(15,5)	(7.058, 215.035)	1	10.443	16.270	2.624	3.337	0.010	0.123	0.000
	(6.691, 203.737)	2	20.886	32.515	6.883	0.211	0.010	0.123	0.015
	(3640, 8976)	3	31.328	48.701	12.648	1.378	0.013	0.111	0.055
(11,11)	(7.459, 223.816)	1	10.103	15.574	2.549	3.303	0.020	0.045	0.430
	(7.071, 211.130)	2	20.206	31.122	6.680	0.187	0.020	0.026	0.403
	(4004, 9706)	3	30.309	46.722	12.263	1.391	0.020	0.221	0.390
(20,0)	(7.830, 238.560)	1	9.346	14.691	2.367	3.304	0.000	0.129	0.713
	(7.422, 222.966)	2	18.691	29.359	6.207	0.233	0.005	0.143	0.672
	(4480, 10704)	3	28.034	43.977	11.402	1.356	0.014	0.175	0.645
(19,3)	(8.090, 264.085)	1	8.464	13.258	2.001	3.349	0.738	0.829	0.908
	(7.666, 250.557)	2	16.928	26.498	5.277	0.225	0.732	0.837	0.841
	(5124, 12299)	3	25.390	39.697	9.760	1.367	0.726	9.163	0.795
(13,13)	(8.815, 265.627)	1	8.484	13.120	2.137	3.299	0.000	0.130	0.280
	(8.355, 250.718)	2	16.969	26.217	5.602	0.193	0.000	0.107	0.267
	(5616, 13554)	3	25.453	39.265	10.288	1.383	0.000	0.071	0.242
(17,9)	(8.953, 292.268)	1	7.689	11.938	1.802	3.329	0.000	0.109	0.167
	(8.485, 277.197)	2	15.379	23.858	4.754	0.203	0.000	0.096	0.147
	(6276, 14958)	3	23.069	35.742	8.796	1.384	0.004	0.078	0.102
(23,0)	(9.004, 272.640)	1	8.177	12.837	2.080	3.301	0.000	0.125	0.288
	(8.534, 255.246)	2	16.354	25.655	5.451	0.230	0.006	0.144	0.147
	(5888, 14025)	3	24.530	38.428	10.009	1.370	0.000	0.172	0.150
(15,15)	(10.171, 309.898)	1	7.255	11.244	1.811	3.302	0.041	0.098	0.275
	(9.640, 292.642)	2	14.511	22.488	4.753	0.198	0.041	0.165	0.063
	(7560, 18166)	3	21.768	33.654	8.738	1.377	0.032	0.054	0.240
(26,0)	(10.179, 315.240)	1	7.073	11.092	1.758	3.301	0.028	0.117	0.114
	(9.646, 295.587)	2	14.145	22.168	4.618	0.228	0.021	0.136	0.108
	(7696, 18352)	3	21.217	33.207	8.500	1.369	0.019	0.151	0.118

^a r and l are the radius and the length of a SWCNT, and subscripts 0 and e refer to the initial and the relaxed configurations, respectively.

^bTorsional mode.

^cAxial mode.

^dBending mode.

^e n_C and N are, respectively, the number of carbon atoms in the SWCNT, and the number of 20-node hexahedral elements into which the equivalent continuum tube is discretized.

^fMode number.

SWCNT and 20-node brick elements in its ECS, frequencies of first three axial, torsional, and bending modes of vibration from the two approaches, and computed values of Young's modulus, Poisson's ratio, and the shear modulus with the wall thickness of 1 Å. It can be concluded that the value of Young's modulus of a SWCNT varies from 3.182 TPa to 3.401 TPa, has mean and median values of 3.312 TPa and 3.303 TPa, and has standard deviation of 0.046 TPa. The largest and the smallest values of E are for the (10,0) and (5,0) SWCNTs, respectively. Young's modulus is independent of the tube diameter and its helicity within an error of 6.4%. With an increase in the diameter of the SWCNT, Poisson's ratio converges to 0.20 for armchair tubes, to 0.23 for zigzag tubes, and to 0.21 for chiral tubes. It varies from the lowest value of 0.144 for the (5,5) SWCNT to the highest value of 0.251 for the (10,0) SWCNT, and the mean, the median, and the standard deviations are, respectively, 0.203, 0.201, and 0.029.

For the SWCNTs studied herein, the frequencies of the first bending mode from MD simulations, Euler's beam theory (EBT) [23], and FE simulations are compared in Table 3 for wall thickness of 1 Å. It is observed that the frequencies from the EBT have on average 3% error as compared with those from MD simulations. If one extracts the thickness by equating the frequencies given by the MD simulations and the EBT then one gets an imaginary value of the wall thickness. However, this is not the case for the thickness computed using the frequencies obtained from the 3D elasticity theory. It suggests that the EBT theory may not be adequate to model the vibrations of SWCNTs. Consequently val-

Table 3 Comparison of frequencies of the first bending mode from 3D-FEA and EBT with those from MD simulations

Tube	Molecular dynamics (cm ⁻¹)	3D-FEA [% error	EBT [% error
(5,0)	9.823	0.657	3.763
(5,5)	5.513	0.595	3.373
(10,0)	4.802	0.249	3.034
(9,6)	3.167	0.095	2.475
(8,8)	3.433	0.464	3.245
(14,2)	3.075	0.033	2.715
(9,9)	3.076	0.453	3.252
(16,0)	2.943	0.271	3.000
(10,10)	2.788	0.393	3.207
(15,5)	2.624	0.000	2.726
(11,11)	2.549	0.430	3.272
(20,0)	2.367	0.713	4.172
(19,3)	2.001	0.908	1.480
(13,13)	2.137	0.280	3.098
(17,9)	1.802	0.167	2.200
(23,0)	2.080	0.288	3.987
(15,15)	1.811	0.275	3.051
(26,0)	1.758	0.114	3.727
Mean % Error		0.355	3.099
Maximum % Error		0.908	4.172

Table 4 Frequencies of radial breathing modes for SWCNTs (N.A.=not available) from MD and 3D-FE simulations, and values reported in literature

Tube	Molecular dynamics (cm ⁻¹)	Present 3D-FEA (cm ⁻¹)	% error with respect to MD results	Rao et al. [16] (cm ⁻¹)	Lawler et al. [17] (cm ⁻¹)	Kurti et al. [18] (cm ⁻¹)	Kuzmany et al. [19] (cm ⁻¹) (Expt.)
(5,0)	568.847	569.857	0.178	N.A.	602	N.A.	N.A.
(5,5)	332.881	328.515	1.312	N.A.	341	N.A.	N.A.
(10,0)	290.463	298.025	2.603	N.A.	294	298	N.A.
(8,8)	209.008	206.493	1.203	206	210	219	211
(14,2)	192.508	194.731	1.155	N.A.	191	N.A.	N.A.
(9,9)	185.896	183.816	1.119	183	187	195	195
(16,0)	181.747	183.790	1.124	N.A.	177	188 (fitted)	185
(10,10)	167.377	165.621	1.049	165	169	175	177
(11,11)	152.207	150.904	0.856	150	N.A.	159	162
(20,0)	145.363	144.598	0.526	N.A.	N.A.	150	N.A.
Maximum % error			2.6				

ues of Young's modulus predicted [25] using experimental frequencies of oscillations coupled with the EBT may not be very reliable.

Frequencies (Hz/speed of light in cm/s) of RBMs computed from the MD and the 3D-FE simulations are listed in Table 4 for $j=1$ along with those reported in literature using theoretical and spectroscopic analyses. It is observed that the frequencies of RBMs for SWCNTs from MD and of ECSs from FE simulations agree well with each other, and are in good agreement with those obtained by other investigators thus validating our computed value of the wall thickness of the ECS. In the absence of geometric details of SWCNTs used in experimental studies one cannot discuss the sources of discrepancy between the simulation and the experimental results. Simulations can incorporate periodic boundary conditions on a unit cell thus mimicking an infinitely long tube, while experiments are conducted with the *finite length* tubes. Therefore it is appropriate in experimental studies that the criterion, $l_e/j \gg r_e$, be met for identifying the frequencies of RBMs. Furthermore, it is observed that *axisymmetric* modes for $j \geq 1$ are closely packed in the phonon spectrum (from both MD and 3D-FE simulations). Therefore the assignment of spectral lines in experiments for RBMs may be difficult and have an error due to not satisfying $l_e/j \gg r_e$. Figure 4 shows *axisymmetric* modes for the (8,8) tube for $j=1$ and 2 from MD and 3D-FE simulations. We note that the experimental value, 211 cm⁻¹, of the frequency of the RBM listed in Table 4 for the (8,8) SWCNT corresponds to the one from simulations with $j > 1$.

Based on the results of compression of a bundle of SWCNTs by external hydrostatic pressure, it has been proposed [7] that the wall thickness of a SWCNT must be less than the theoretical diameter of a carbon atom (1.42 Å). Our work based on dynamical quantities predicts the wall thickness to be ~ 1 Å.

4 Remarks

The values of Young's modulus, the shear modulus, and Poisson's ratio computed herein from MD simulations of vibrations differ from those reported by other investigators mainly due to the different value of the wall thickness. Whereas we have deduced the value of the thickness of the ECS by equating the frequencies

of bending modes of vibration, most other studies have assumed it a priori. Using MM simulations with the MM3 potential, Sears and Batra [22] found that for the (16,0) SWCNT

$$E = \frac{1.18 \times 10^{-6}}{2\pi r_e h} \text{Pa}$$

where h is the wall thickness of the ECS. Substitution for $r_e = 5.939$ Å and $h = 1$ Å gives $E = 3.162$ TPa, which compares well with the 3.36 TPa obtained herein. Thus simulations of static deformations and vibrations give values of E with a difference of 6%. The values of G for the (16,0) SWCNT computed from Sears and Batra's [22] MM simulations and our present work are 1.298 TPa and 1.356 TPa, respectively, and have a difference of about 4.3%.

Whereas we have derived the elastic moduli of the ECS by comparing the results of MD simulations with those of FEA using the 3D elasticity theory for isotropic materials, Huang et al. [26], Wu et al. [27], and Peng et al. [28] have used the Brenner potential to derive elastic properties of a nonlinear elastic shell and found its stiffness in tension, bending, and torsion. They have also studied deformations of the shell due to radial loads applied on the inner and on the outer surfaces of the shell, and its buckling due to axial loads. The Brenner potential includes energies due to bond stretching, and bending induced by changes in angles between adjacent bonds. They [26–28] have shown that the material of the shell should be modeled as orthotropic. For atomic spacing, Δ , tube radius, R , and characteristic length of the continuum structure, L , they [26–28] have estimated errors in the results from shell theories as a function of Δ/R and Δ/L . For the SWCNTs studied herein, $\Delta/L \sim 15$ and the error in the ECS is only a function of Δ/R . For the error to be of $O[(\Delta/R)^3]$, a SWCNT cannot be represented by a conventional shell theory because constitutive relations involve coupling between tension and curvature, and between bending and axial strain. For the error to be $O[(\Delta/R)^2]$, the tension and bending rigidities of SWCNTs can be represented by an elastic orthotropic thin shell, but not by the thickness and the elastic modulus. Only for the error of $O[(\Delta/R)]$, a universal constant shell thickness can be defined and a SWCNT can be modeled as a thin shell of uniform thickness and made of an isotropic elastic material. In the present work, we have used FEA results from the 3D linear elasticity theory of isotropic materials to deduce the elastic moduli and the uniform thickness of the ECS. Also, the MM3 potential includes energies due to torsion, and coupling between twisting and stretching, bending and stretching, and van der Waals forces. Thus, it is not easy to estimate errors in the linear elastic cylindrical tube comprised of an isotropic elastic material that is equivalent to the SWCNT.

Batra and Sears [29] proposed that the ECS of a SWCNT be a cylindrical tube of mean radius equal to that of the SWCNT, and

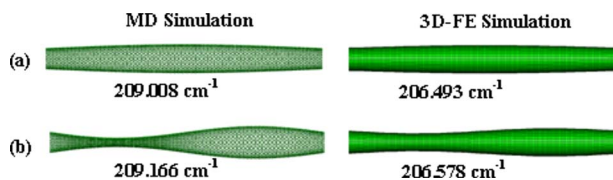


Fig. 4 Radial breathing modes of free-free (8,8) SWCNT corresponding to (a) $j=1$ and (b) $j=2$

be made of a transversely isotropic material with the axis of transverse isotropy along the radial direction. They studied the radial deformations of the ECS and of the SWCNT due to pressures applied on the inner and on the outer surfaces, and found that Young's modulus in the radial direction is nearly one-fourth of that in the axial direction. If a similar assumption were made here, then the presently computed value of E is for Young's modulus in the axial and circumferential directions, and the values of Poisson's ratio and the shear modulus in the θz -plane have been found. Here z -axis is along the axis of the tube and θ denotes the angular position of a point. In the vibration modes studied, displacements only in one direction are dominant. However, we cannot find the remaining two elastic moduli of the transversely isotropic linear elastic material from the vibration modes studied here.

We note that Wang and Zhang [30] have recently summarized the values of wall thickness of a SWCNT obtained by different research groups. Also, Sears and Batra [31] have used the MM3 potential to study buckling, due to axial compression, of single- and multi-walled CNTs.

5 Conclusions

We conclude that SWCNTs of different chiralities can be regarded as $\sim 1 \text{ \AA}$ thick with the axial Young's modulus of between 3.2 TPa and 3.4 TPa with a standard deviation of 0.046. The values of Poisson's ratio range between 0.144 and 0.251, and their mean and standard deviations are 0.203 and 0.029, respectively. The frequencies of radial breathing modes of tubes of different helicities from MD and 3D-FEA simulations are found to agree well with each other with a maximum difference of 2.6%. These are close to those derived by other researchers either from quantum mechanical simulations or experimental studies. The results presented herein have important consequences in designing SWCNT based nanodevices.

Acknowledgment

This work was supported by the Office of Naval Research Grant No. N00014-98-06-0567 to Virginia Polytechnic Institute and State University with Dr. Y.D.S. Rajapakse as the program manager. Financial support from Virginia Tech's Institute of Critical Technologies and Sciences is gratefully acknowledged.

References

- [1] Ijima, S., 1991, "Helical Microtubules of Graphitic Carbon," *Nature (London)*, **354**, pp. 56–58.
- [2] Yakobson, B. I., Brabec, C. J., and Bernholc, J., 1996, "Nanomechanics of Carbon Tubes: Instabilities Beyond Linear Response," *Phys. Rev. Lett.*, **76**, pp. 2511–2514.
- [3] Zhou, X., Zhou, J., and Ou-Yang, Z., 2000, "Strain Energy and Young's Modulus of Single-Walled Carbon Nanotubes Calculated From Electronic Energy-Band Theory," *Phys. Rev. B*, **62**, pp. 13692–13696.
- [4] Kudin, K. N., Scuseria, G. E., and Yakobson, B. I., 2001, " C_2F , BN, and C Nanoshell Elasticity From *Ab Initio* Computations," *Phys. Rev. B*, **64**, p. 235406.
- [5] Tu, Z. C., and Ou-Yang, Z., 2002, "Single-Walled and Multiwalled Carbon Nanotubes Viewed as Elastic Tubes With the Effective Young's Moduli Dependent on Layer Number," *Phys. Rev. B*, **65**, p. 233407.
- [6] Reich, S., Thomsen, C., and Ordejon, P., 2002, "Elastic Properties of Carbon Nanotubes Under Hydrostatic Pressure," *Phys. Rev. B*, **65**, p. 153407.
- [7] Vodenitcharova, T., and Zhang, L. C., 2003, "Effective Wall Thickness of a Single-Walled Carbon Nanotube," *Phys. Rev. B*, **68**, p. 165401.
- [8] Pantano, A., Parks, D. M., and Boyce, M. C., 2004, "Mechanics of Deformation of Single- and Multi-Wall Carbon Nanotubes," *J. Mech. Phys. Solids*, **52**, pp. 789–821.
- [9] Wang, L., Zheng, Q., Liu, J. Z., and Jiang, Q., 2005, "Size Dependence of the Thin-Shell Model for Carbon Nanotubes," *Phys. Rev. Lett.*, **95**, p. 105501.
- [10] Chen, X., and Cao, G., 2006, "A Structural Mechanics Study of Single-Walled Carbon Nanotubes Generalized From Atomistic Simulation," *Nanotechnology*, **17**, pp. 1004–1015.
- [11] Wu, Y., Xiang, X., Leung, A. Y. T., and Zhong, W., 2006, "An Energy-Equivalent Model on Studying the Mechanical Properties of Single-Walled Carbon Nanotubes," *Thin-Walled Struct.*, **44**, pp. 667–676.
- [12] Kalamkarov, A. L., Georgiades, A. V., Rokkam, S. K., Veedu, V. P., and Ghasemi-Nejhad, M. N., 2006, "Analytical and Numerical Techniques to Predict Carbon Nanotubes Properties," *Int. J. Solids Struct.*, **43**, pp. 6832–6854.
- [13] Halicioglu, T., 1998, "Stress Calculations for Carbon Nanotubes," *Thin Solid Films*, **312**, pp. 11–14.
- [14] Yu, M.-F., Lourie, O., Dyer, M. J., Moloni, K., Kelly, T. F., and Rodney, S. R., 2000, "Strength and Breaking Mechanisms of Multiwalled Carbon Nanotubes Under Tensile Load," *Science*, **287**, pp. 637–640.
- [15] Ray, M. C., and Batra, R. C., 2007, "A Single-Walled Carbon Nanotube Reinforced 1-3 Piezoelectric Composite for Active Control of Smart Structures," *Smart Mater. Struct.*, **16**, pp. 1936–1947.
- [16] Rao, A. M., Richter, E., Bandow, S., Chase, B., Eklund, P. C., Williams, K. A., Fang, S., Subbaswamy, K. R., Menon, M., Thess, A., Smalley, R. E., Dresselhaus, G., and Dresselhaus, M. S., 1997, "Diameter-Selective Raman Scattering From Vibrational Modes in Carbon Nanotubes," *Science*, **275**, pp. 187–191.
- [17] Lawler, H. M., Areshkin, D., Mintmire, J. W., and White, C. T., 2005, "Radial-Breathing Mode Frequencies for Single-Walled Carbon Nanotubes of Arbitrary Chirality: First-Principle Calculations," *Phys. Rev. B*, **72**, p. 233403.
- [18] Kurti, J., Kresse, G., and Kuzmany, H., 1998, "First-Principles Calculations of the Radial Breathing Mode of Single-Wall Carbon Nanotubes," *Phys. Rev. B*, **58**, pp. R8869–8872.
- [19] Kuzmany, H., Burger, B., Hulman, M., Kurti, J., Rinzler, A. G., and Smalley, R. E., 1998, "Spectroscopic Analysis of Different Types of Single-Wall Carbon Nanotubes," *Europhys. Lett.*, **44**, pp. 518–524.
- [20] Allinger, N. L., Yuh, Y. H., and Lii, J. H., 1998, "Molecular Mechanics. The MM3 Force Field for Hydrocarbons," *J. Am. Chem. Soc.*, **111**, pp. 8551–8566.
- [21] Ponder, J. W., 2004, User's Guide TINKER Molecular Modelling Package 4.2.
- [22] Sears, A., and Batra, R. C., 2004, "Macroscopic Properties of Carbon Nanotubes From Molecular-Mechanics Simulations," *Phys. Rev. B*, **69**, pp. 235406.
- [23] Blevins, R. D., 1979, *Formulas For Natural Frequencies and Mode Shapes*, Van Nostrand Reinhold, New York.
- [24] User's Manual Finite Element Computer Code ABAQUS 6.6.
- [25] Krishnan, A., Dujardin, E., Ebbesen, T. W., Yianilos, P. N., and Treacy, M. M. J., 1998, "Young's Modulus of Single-Walled Nanotubes," *Phys. Rev. B*, **58**, pp. 14013–14019.
- [26] Huang, Y., Wu, J., and Hwang, K. C., 2006, "Thickness of Graphene and Single-Wall Carbon Nanotubes," *Phys. Rev. B*, **74**, pp. 245413.
- [27] Wu, J., Hwang, K. C., and Huang, Y., 2008, "An Atomistic-Based Finite-Deformation Shell Theory for Single-Wall Carbon Nanotubes," *J. Mech. Phys. Solids*, **56**, pp. 279–292.
- [28] Peng, J., Wu, J., Hwang, K. C., Song, J., and Huang, Y., 2008, "Can a Single-Wall Carbon Nanotube be Modelled as a Thin Shell?," *J. Mech. Phys. Solids*, to be published.
- [29] Batra, R. C., and Sears, A., 2007, "Uniform Radial Expansion/Contraction of Carbon Nanotubes and Their Transverse Elastic Moduli," *Modell. Simul. Mater. Sci. Eng.*, **15**, pp. 835–844.
- [30] Wang, C. Y., and Zhang, L. C., 2008, "A Critical Assessment of the Elastic Properties and Effective Wall Thickness of Single-Walled Carbon Nanotubes," *Nanotechnology*, **19**, p. 075705.
- [31] Sears, A., and Batra, R. C., 2006, "Buckling of Multi-Walled Carbon Nanotubes Under Axial Compression," *Phys. Rev. B*, **73**, p. 085410.